Synchrotron Radiation News

ISSN: 0894-0886 (Print) 1931-7344 (Online) Journal homepage: https://www.tandfonline.com/loi/gsrn20

First NanoARPES User Facility Available at SOLEIL: An Innovative and Powerful Tool for Studying Advanced Materials

José Avila & María C. Asensio

To cite this article: José Avila & María C. Asensio (2014) First NanoARPES User Facility Available at SOLEIL: An Innovative and Powerful Tool for Studying Advanced Materials, Synchrotron Radiation News, 27:2, 24-30, DOI: 10.1080/08940886.2014.889549

To link to this article: https://doi.org/10.1080/08940886.2014.889549

Copyright Taylor & Francis

Published online: 24 Mar 2014.

Submit your article to this journal

Article views: 1921

View related articles

View Crossmark data

Citing articles: 17 View citing articles

Full Terms & Conditions of access and use can be found at
https://www.tandfonline.com/action/journalInformation?journalCode=gsrn20

First NanoARPES User Facility Available at SOLEIL: An Innovative and Powerful Tool for Studying Advanced Materials

José Avila and María C. Asensio
Synchrotron SOLEIL, Gif-sur-Yvette, France

During the last few decades, many scientific research areas have experienced remarkable progress in nanoscience and nanotechnology. In an even rather wider field, complex and smart materials are also often isolated as small crystallites, and they present serious difficulties in terms of being synthesized without fluctuations of their compositions or crystalline orientations. This particular interest in material characterization at rather small scales has considerably affected the design, manufacturing, and performance of advanced scientific instruments. In fact, when characterizing advanced materials, progress frequently refers to a new area of knowledge, to the need of seeing, measuring, and understanding objects at the nano- and mesoscopic scale.

Overcoming the critical step in the manufacture of nano-objects or complex materials, even if these "smart-units" have remarkable properties, they would have remained unexploited if new tools have not been developed for analyzing and measuring those objects on a wide range of scales, from a few microns to tens of nanometers. Hence, precise and fine electronic and compositional characterization is revealed to be rather intricate if the novel materials are affected by phase separation, such as doped Mott insulators or magnetic domains, composites with nano- or micro-crystallites embedded in isolating and flexible host materials, as well as nano- or micro-patterned objects, among others.

Recently, a tremendous and fast expansion in modern microscopic methods has been realized. However, beyond the achievement of Angstrom spatial resolution, the challenge still remains in order to consolidate energy-resolved spectroscopic methods with lateral nanometric resolution. A fine chemical and electronic analysis with submicron spatial discrimination has been revealed to be indispensable for many scientific problems. X-ray scanning spectromicroscopy, both photoelectron and X-ray absorption, is a technique based on high brilliant tuneable synchrotron radiation (SR) sources, particularly well positioned to provide both spatial resolution and chemical sensitivity.

Traditionally, these techniques have guaranteed chemical imaging by taking advantage of the spatial contrast created by X-ray absorption and the intensity variation of core-level photoelectrons, giving rise to X-ray scanning transmission microscopy (SXTM) and scanning photoelectron microscopy (SPEM), respectively. In both cases, the Fresnel Zone Plates (FZPs) performance, varying from micrometer to nanometric lateral resolution, is the determinant and essential component. Nowadays, several companies in the market provide FZPs with resolution better than 30 nm, which has facilitated the construction and operation of several such scanning microscopes in different synchrotron radiation facilities like Elettra, ALS, CLS, and MAX-lab, among others.

In the scanning X-ray photoelectron microscope approach, the X-ray photon optics focalizes the incident photon beam to a small spot onto the sample, obtaining the image by detecting the emitted photoelectrons while rastering the sample in front of the demagnified photon beam. In spite of the enormous success of the well-established scanning photoelectron microscope (SPEM) technique, it has been shown that a similar lateral resolution for recording the band electronic structure of complex materials and nano-objects could have determinant repercussions on the comprehension of a wide variety of fundamental mechanisms.

The main goal then is to follow the implication of heterogeneities and confinement on the delocalized or partially localized electronic states. For such an aim, the description of the electronic structure must be complete, not only with regard to the core-level detection, but also taking into account those states typically present close to the Fermi level, with no more than 15–20 eV of binding energy. This objective is rather pertinent as those electronic states are directly responsible for the chemical bonds, reactivity, electrical transport, as well as the thermal, magnetic, and mechanical properties of matter.

However, due to the steric hindrance between standard focalizing zone plates and the photoelectron detectors, the implementation of the scanning photoelectron technique in the low photon energy range ($h\nu < 150$ eV) has been considered impractical for a long time. In particular, a potential project where the nanometer lateral resolution could be combined with typical angle-resolved photoelectron spectroscopy (ARPES) measurements has been considered by many experts to be fully unreasonable, taking into account the demanding requirements of the angular degree of freedom associated with classical ARPES experiments.

Nevertheless, the accessibility of new, low-emittance SR storage rings equipped with long insertion devices and accurate electron orbits control has contributed to the idea that third-generation synchrotron soft X-ray radiation facilities could be considered as excellent candidates for developing spectroscopy in the domain of microscopy. Hence, the ultra-high brightness of these sources makes it possible to bring together two very demanding techniques, like ARPES and scanning

photoemission microscopy. This combination is able to register the dispersive energy-momentum spectrum (by angular-resolved photoemission) on micro- and nano-samples as well as performing "electronic imaging" by recording the valence band states with high energy, angular and spatial resolution. We present here the main conceptual design of the beamline and end-station, together with some recent commissioning and scientific results.

Layout of the facility and its performance

As one of the latest beamlines built at the SOLEIL synchrotron source, ANTARES instrumentation offers a spectroscopic non-destructive nano-probe to study advanced materials. This innovative scanning photoemission microscopy combines linear and angle sweeps to perform precise electronic band structure determination by nanoARPES and chemical imaging with core-level detection. The design effectively integrates insertion devices together with high transmission optics (see Figure 1). This photon source has been combined with an advanced microscope which has precise sample handling abilities. Moreover, it is fully compatible with the high angular and energy resolved R4000 Scienta hemispherical analyzer and a set of Fresnel Zone Plates (FZP) is able to focalize the beam spot up to a few tens of nanometers, depending on the spatial resolution of the selected FZP.

The whole optics system of the ANTARES beamline has been outlined as a robust instrument entirely optimized to illuminate the focalizing lens (the FZPs) of the photoelectron microscope without losing a high flexibility in selecting monochromatic light over a large photon energy range. As the source of photons, ANTARES uses a set of two complementary insertion devices (H60 and H256 undulators) in a tandem configuration, delivering a well-established wide spectral distribution with discriminated circular and linear polarization [1]. Moreover, a low-level, fully automatic software system allows a rapid and precise selection of the wavelength at the monochromator and the undulator harmonic of highest flux for each selected working energy. Most importantly, the beamline optics ensures an excellent match between the set of two undulators and the varied-line-spacing (VLS) plane-grating monochromator (PGM). The combination of these two essential elements provides a source of intense circularly and linearly polarized light from the ultraviolet to the soft X-ray spectra, which ranges from 10 eV up to 1000 eV. The beamline presents a performance according to its specifications, with high positioning reproducibility, and thermal and mechanical stability [1, 2].

Furthermore, the ANTARES beamline benefits, like the other SOLEIL beamlines, from the extremely stable operation conditions of the SOLEIL machine, operating in top mode since 2009. The top-up functioning mode keeps the electron current in the storage ring constant at 400.5 (±0.5) mA, ensuring a constant heat load and consequently minimal thermal drifts within the storage ring and associated optics of the beamlines. Taking advantage of the lamellar gratings with VGD, the ANTARES beamline combines a high resolving power, an excellent harmonic rejection ratio, and a high flux throughout the working energy

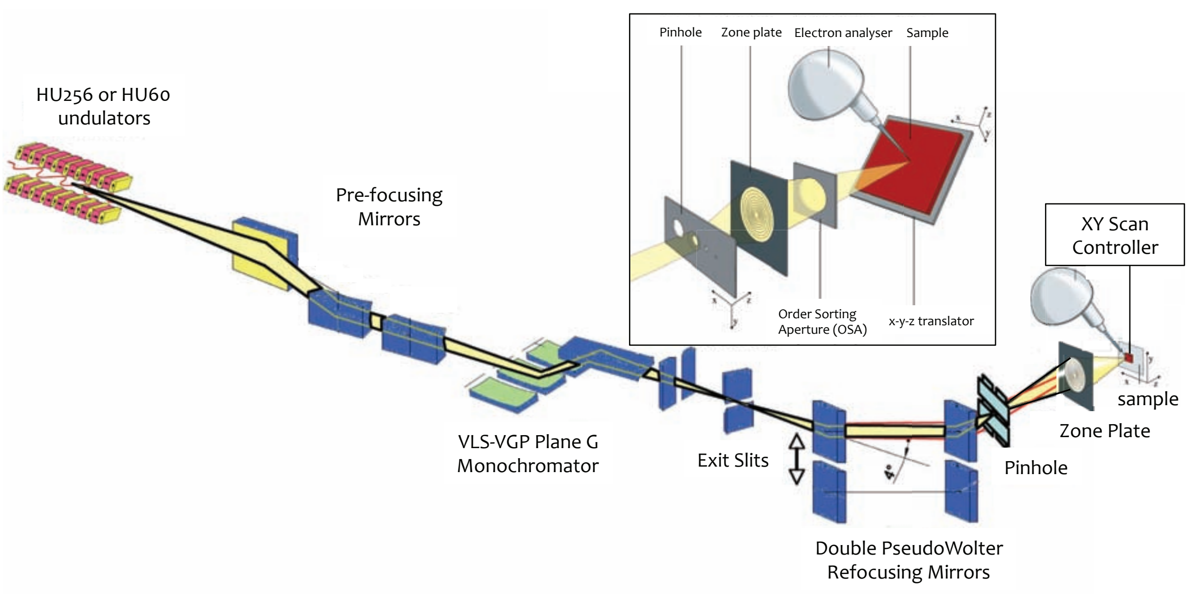

Figure 1: Schematic representation of the basic components of the ANTARES beamline. The first pre-focusing mirrors collimate the undulators beam to a plane-grating monochromator with two gratings that can be exchanged by remote control. The second set of mirrors, or pseudo Wolter post-localization mirrors, refocuses the beam alternatively onto the sample or the pinhole, depending on if a micro- or a nanometer spot size is required. The FZP focusing system is also included in the NanoARPES endstation, together with an order selection aperture (OSA) placed between the FZP and the sample, in order to suppress unwanted diffraction orders. The inset shows in detail the essential components of the ANTARES microscope together with the high-angular and high-energy-resolution Scienta R4000 photoelectron detector.

range, which is particularly compatible with the extremely demanding use of FZPs. Typically, the photon flux on the sample is 6.4×10^{12} photons/sec/0.01% BW working in micro-spot mode and 5.4×10^{10} photons/sec/0.01% BW for nano-spot experiments, with a standard resolving power of 32000 at 67 eV photon energy.

The experimental end-station is equipped with an analysis chamber containing the microscope, a preparation chamber with gas lines, and a fast entry chamber that allows a fast sample transfer from atmospheric to ultra-high-vacuum conditions. The hutch accommodates the pinhole chamber and the analysis chamber, which contains the electron analyzer and nano-spot focusing optics. In order to ensure a precise nanometer scanning of the sample, both the thermal drift and the mechanical vibrations are minimized by an interferometric control. The thermal variation is stabilized to be lower than 0.1°C and the mechanical vibrations are minimized to have only spurious displacements, which are compensated for by the interferometric system.

The main difference between the ANTARES microscope and other conventional ARPES instruments is that the specimens are mounted on a high-precision plate that ensures their nanoscale positioning in the x, y, and z directions. The polar angle (Θ) and the azimuthal angles (Ψ) can also be automatically scanned over a 90° range. Finally, the soft X-ray beam with a controlled linear or circular polarization can be focused to about 30 nm (or better), depending on the quality of the FZP lenses used. The ANTARES microscope has two operating modes, spectroscopy with nano-spot and spectroscopic imaging.

As the aim of the project is to attain nanometer resolution, the nanoARPES microscope is equipped with a continuous interferometric control of the position of the samples with respect to the FZPs, which avoids thermal and mechanical drifts, preventing undesirable distortions of the recorded images. Thus, the accurate real-time recording of the location of the X-ray spot on the sample by interferometry is automatically converted into a digital signal that controls by a feedback closed-loop the scanning positioning of the specimen.

Selected results and application examples

Taking advantage of this innovative facility, a wide variety of experiments have already been carried out on many interesting materials since the beginning of user operation a few years ago. Here we present some examples that, far from being an exhaustive list, will give a flavor of the type of problems that can be successfully tackled by the nano-ARPES user facility available at the SOLEIL synchrotron.

Semiconductor nano-wires have shown promising properties for many device applications, but controlled doping with electronic impurities remains an important challenge. Limitations on dopant incorporation have been identified in nano-crystals, raising concerns about the prospects for doping other nanostructures. In addition, progress has been hindered by the lack of methods to quantify the dopant distribution in single nanostructures. Nano-photoemission can, in principle, allow performing non-destructive microscopic analysis of the chemical composition and electronic structure of single nano-wires. Such quantified information could have important implications for controlling the incorporation of impurities in semiconductor nano-wires and for turning them into electrically active dopants.

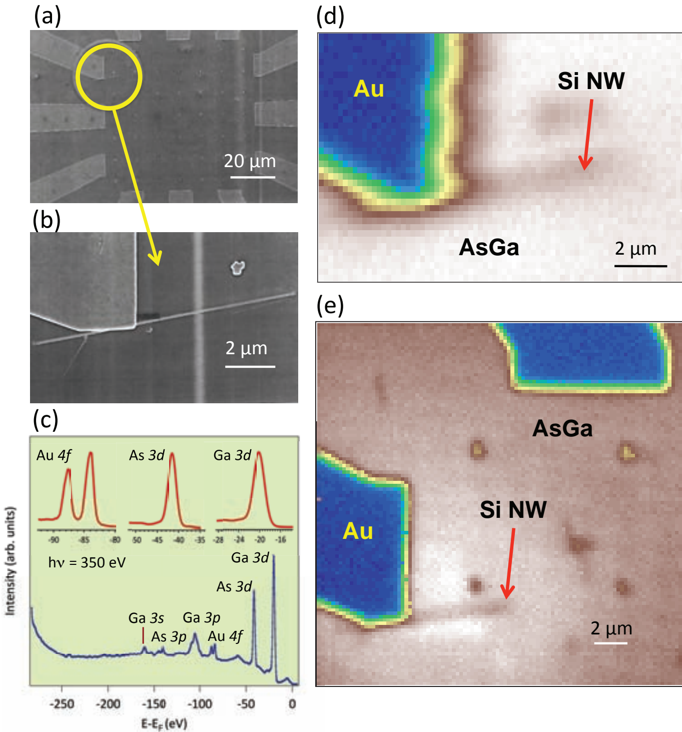

Figure 2: Characterization by micro- and nano-XPS of silicon nano-wires on a GaAs substrate patterned with gold. Panels (a) and (b) show SEM images of the sample and the silicon nano-wire connected by gold legs. Panel (c) displays a micro-XPS overview spectrum with significant signal of Au (4f), As (3d), and Ga (3d)) core levels. Top insets of the panel show individual core-level spectra measured using nano-XPS. The spectra have been all recorded using hν = 350 eV. Panels (d) and (e) show real-space two-dimensional images of the elemental distribution of the patterned sample by monitoring the area of the As (3d) core-level spectrum, indicated in the inset of panel (c).

Valence band and core-level measurements of isolated nano-objects such as boron-doped silicon nano-wires have been carried out recently at the ANTARES beamline, with a spatial resolution better than 100 nm. Figure 2 shows one of these silicon nano-wires connected to gold legs on a GaAs-patterned substrate. In panel (a), a secondary electron microscopy (SEM) image of this sample depicts its characteristic pattern with 12 gold legs and small gold dots that act as markers of different areas of the sample. Panel (b) illustrates a zone of panel (a) where a single nano-wire can be identified. A survey photoemission spectrum recorded using a large photon spot of ~90 µm (micro-XPS) of this patterned sample comprehensibly indicates the presence of gallium, arsenic, and gold, revealed by significant signal of Au (3d), As (3d), and Au (4f) core levels. However, this spectroscopic information is totally insensible to the patterning of the sample and it is not even able to detect the small signal due to the presence of little concentration of nano-wires in the investigated sample (see panel (c)).

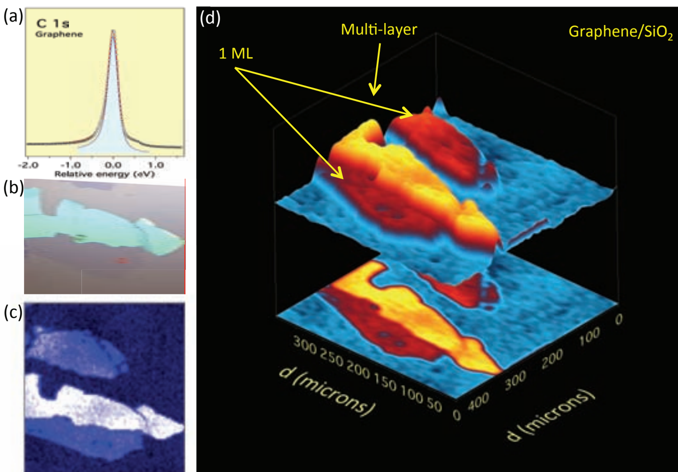

Figure 3: Nano-XPS results on exfoliated graphene samples on SiO_2 substrates recorded at the ANTARES beamline. Panel (a) shows C1s core level recorded with a nano-spot of ~100 nm size using hν = 350 eV photon energy in the area of the sample that corresponds to one-atom tick graphene film. The reference binding energy is 284.5(±5) eV. Panel (b) displays an optical micrograph of the high-quality exfoliated graphene single crystal transferred onto an isolated SiO_2 substrate. Panels (c) and (d) show two- and three-dimensional nano-XPS imaging of the C1s intensity displayed in panel (a).

The top- and bottom-right panels show the same type of spectroscopic information displayed in Figure 2c, but as two-dimensional images, taking advantage of the precise sample scanning and focalized nano-spot performance of the ANTARES microscope. The nano-XPS image of panel (d) shows one of the gold legs connected to the silicon nano-wire, using a spot size of ~100 nm. Despite the fact that the image is clear due to the lack of interferometer control during these measurements, the contrast of the image is rather poor and spurious distortions are observed, particularly evident in the straight areas of the patterned sample; for example, the front part of the main gold leg. As soon as the real-time interferometric feedback closed-loop is included in the measurements, the obtained images are free of thermal drifts and mechanical vibrations, as can be seen in Figure 2e.

The bottom-right panel of Figure 2e shows the same area of the sample of panel (d), but with much better contrast and spatial resolution and free of thermal drift distortions. The resulting nano-XPS image plots the intensity of the selected core level (in this case, As 3d) as a function of x and y positions of the nano-spot on the sample. As is shown on the inset of the panel of Figure 2c, the Scienta spectrometer is able to record almost simultaneously the intensity of all characteristic core levels present in the sample investigated; i.e., in this case, Au (4f), As (3d), Ga(3d), and Si (2p). Thus, from one unique sample scanning, independent images can be generated, plotting the intensity of each recorded core level as a function of the sample position, describing thus the quantitative distribution of each element present in the investigated specimen.

Figure 3 shows the same type of nano-XPS results, this time monitoring the intensity of C1s core level of an exfoliated graphene sample deposited on an SiO_2 substrate. The real-space image displaying the intensity of the C1s core level is shown in Figure 3d. The two-dimensional distribution of the graphene C1s core level (Figure 3a) allows the localization and determination with high precision of the extension of one-atom-thick layer, bilayer, and multilayer graphene areas after the exfoliation and transfer of the graphene to the isolated SiO_2 substrate. The three-dimensional representation of the C1s core-level intensity in panel (d) displays clearly the extension and different thicknesses of the exfoliated graphene, showing the shape of the sample fully concordant with its optical micrograph depicted in panel (b).

Even if element-specific images like the ones presented in Figures 2 and 3 are quite advantageous, providing useful chemical and compositional information of rather small samples, the X-ray focalization using FZP in the range of photon energies higher than hν = 350 eV is not a very demanding technique. Depending on the diameter of the FZP utilized, the work distances between the FZP and the samples are generally larger than several centimeters, so rather compatible with voluminous photoelectron spectrometers like Scienta R4000.

However, as soon as the photon energy is lowered, allowing work in the energy range where the cross-section of the valence band states is high (i.e., close to the Fermi level), the instrumental requirements become much more challenging. Figure 4 shows an example where one exfoliated graphene sample transferred to a SiO_2 substrate has been investigated using nanoARPES. The study is very similar to the one we have recently carried out on one-atom-thick graphene films grown on copper foils by chemical vapor deposition [4, 5], where our interest has been centered on the characterization of the robustness of the Dirac relativistic-like electronic spectrum as a function of the size, shape, and orientation of the single-crystal pristine grains (of ~2–4 μm) in the graphene films investigated.

Also, graphene multilayer samples grown by sublimation on silicon- and carbon-terminated SiC substrates [6] have been investigated in ANTARES in order to unravel the problem associated with the eventual different stacking order of individual carbon layers. In particular, epitaxial graphene grown on C-face SiC has for quite some time been claimed [7, 8] to be fundamentally different compared to graphene grown on Si-face SiC. A rotational disorder between adjacent layers has been reported and suggested to explain why classical ARPES results from multilayer C-face graphene exhibited a single π-band cone [9], the characteristic of monolayer graphene. Here also, by nanoARPES mapping of individual μm-sized grains, we could clearly unravel the conical band dispersions close to the Dirac point of single and multilayer graphene as well as the verification of the characteristic Bernal (AB) stacking within grains [10].

Similarly, nanoARPES mapping and E vs $k_{//}$ data close to the Fermi level on exfoliated graphene transferred to an isolated SiO2 substrate are shown in Figure 4. Bearing in mind that the description of collective electronic excitations is essential for many open issues in graphene physics, the ability to perform nanoARPES experiments with high-en-

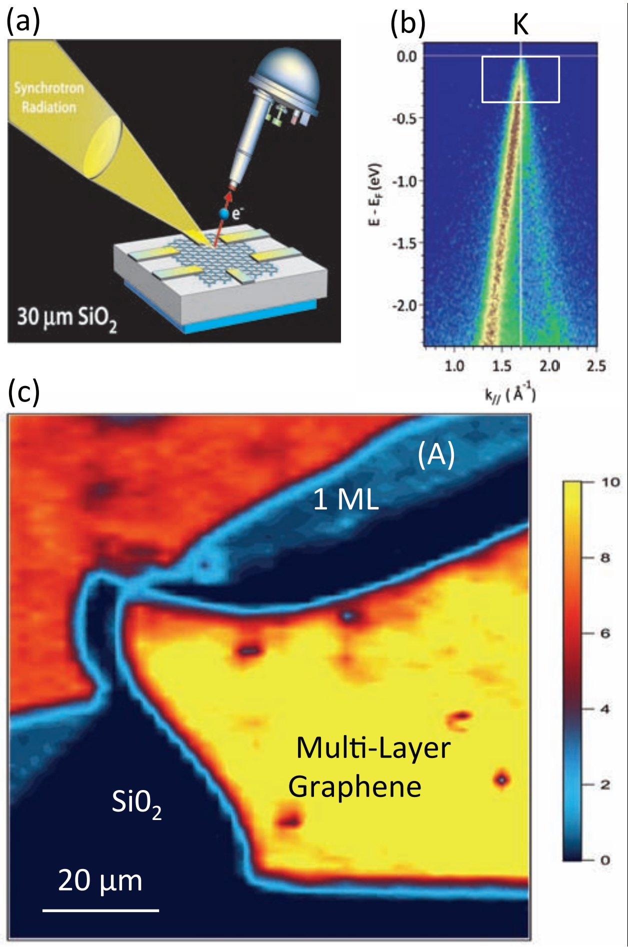

Figure 4: Real-space image and nanoARPES electronic band dispersion close to the Dirac point of the single- and multi-layer graphene films on SiO_2 substrate. (a) Scheme of the nanoARPES apparatus describing the set-up to manipulate micro samples together with the detector set-up (the scale is not respected); (b) nanoARPES data at the labelled "A" position indicated in the image of panel (c). NanoARPES mapping is presented on a linear scale as a false-color image in panel (c). This real-space image represents the intensity variation of the graphene states with a selected $k_{//}$ and binding energy values (states confined in the white box of panel (b)), close to K symmetry point of the graphene Brillouin zone.

ergy, momentum, and lateral resolution on micro- and nano-sized samples allows us to determine the lateral dependence of relevant features like gap-size, doping, effective mass, Fermi velocity, and phonon coupling, among other relevant properties. These fine electronic structure descriptions are essential to resolve important fundamental and applied problems related to layer, bilayer, and multilayer as well as boundary grain issues of low-dimensional, nano- and micro-sized samples.

Finally, Figure 5 presents a complete nanoARPES study of highly pyrolytic-oriented graphite (HOPG) samples, which despite their apparent homogeneity are composed of micrometric single-crystal grains. The samples are poly-crystals composed of micrometer-sized grains of graphite single crystals randomly oriented in the basal plane of the crystal. Hence, the unit cell of HOPG is identical to the graphite single crystal if the random orientation of the individual grains is not taken into account. Each layer of the HOPG grains is composed of carbon atoms arranged in a hexagonal lattice, where the sp^2 electrons are bonded by strong σ covalent bonds and covalent π bonds for the other p electrons. The π bands are fully delocalized bands, perpendicular to the atomic plans, and are responsible for the high electrical and thermal conductivity of graphite (see Figure 5b).

A two-dimensional nanoARPES image of a typical HOPG sample is shown in Figure 5a. The image represents in a linear scale as a false color the intensity of the HOPG π-bands in the energy range 0 to 0.5 eV below the Fermi level and at the $\bar{K}$-point (see Figure 5b, where the high symmetry points of the reciprocal space unit cell of graphite are indicated). Hence, by collecting exclusively the π-states (those confined in the yellow box of Figure 5f), the localization, shape, and orientation of the graphite grains in the HOPG crystal can be precisely determined. As the graphite π- and π*-bands are only close to the Fermi level at the K symmetry points of the grains investigated, the nanoARPES images like the one displayed in Figure 5a detect not only the presence of the single-crystal graphite grains in the HOPG crystal, but also their orientation; i.e., only those grains whose ΓK directions are collinear with the spectrometer energy window are detected. Accordingly, each nanoARPES image provides the size and distribution of the graphite grains with a particular orientation in the HOPG crystals investigated. Most importantly, once the individual single-crystal grains have been identified, we could investigate the electronic properties associated with each individual grain by carrying out punctual nanoARPES measurements inside the localized grain.

The thermal and mechanical stability of the nanoARPES microscope ensures images with strong contrast and highly reproducible. The visualization of each grain, of ~4–10 microns size, is direct and fast. The nanospot punctual mode of nanoARPES allows us to perform a full spectroscopic electronic band dispersion determination, as shown in Figure 5f, where the almost conical dispersion of the HOPG π-bands can be clearly observed. This type of nanoARPES data can be recorded not only inside the grains but also in the grain boundary, where the influence of the border effects on the electronic structure can be investigated.

An alternative way to study the electronic band dispersions of the studied materials is by analyzing photoelectron intensity maps at constant energy. These maps are particularly relevant when they are recorded at the Fermi level, whose energy separates the occupied from the unoccupied bands. However, this determination is quite demanding instrumentally, because it requires very precise angular scanning and an almost perfect coincidence of the light source nano-spot (or position of the FZPs), the Scienta analyzer focus, and the mechanical axis of rotation of the microscope. Moreover, the region of the sample to be measured, in this case the single-crystal graphite grains of not more than a few micrometers size, should be positioned precisely in this coincidence focus of the detection system in order to ensure that the signal is originated always from the same small graphite grain. Figure 5c

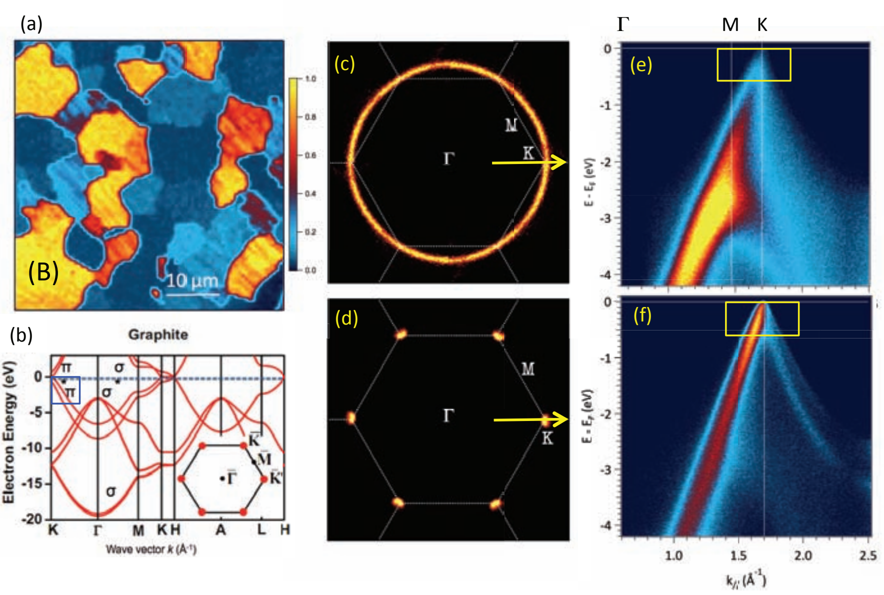

Figure 5: NanoARPES results on HOPG samples obtained with the ANTARES microsope. Panel (b) shows the theoretical electronic structure of graphite single crystal. Panel (a) shows a real-space x-y map of HOPG grains obtained recording the states confined in the yellow box of panel (f). The image obtained using nanoARPES mapping is presented on a linear scale as a false-color plot. Panels (c) and (d) show the Fermi surface of a HOPG sample recorded with micro- and nano-spot, respectively. In panel (d), nanoARPES data has been recorded inside the grain labelled "B" in panel (a). Panels (e) and (f) display punctual recording mode micro- and nanoARPES data corresponding to a multi- and single-grain sampling, respectively.

shows the dominant features of the Fermi surface mapping of a typical HOPG crystal measured using classical high-energy resolution ARPES. The Fermi surface is defined by the intensity of the electronic states at the Fermi level as a function of the azimuthal angle. As in classical micro-spot ARPES, several grains are simultaneously recorded, and the Fermi surface is characterized by a continuous circle of ΓK radius (i.e., 1.7 $Å^{-1}$ of the reciprocal space). The same Fermi surface recorded by nanoARPES is represented in Figure 5d. As the Fermi surface is now recorded collecting the states corresponding only to one single grain of graphite in the HOPG crystal, the main features defining the Fermi surface are only six small pockets of electronic states concentrated at the six corners of the Brillouin zone of graphite.

Conclusions and outlook

In summary, we have presented some relevant examples describing the current performance of the new nanoARPES user facility recently built at the SOLEIL synchrotron. It offers a spectroscopic nano-probe to study complex materials able to image selected electronic states with precise binding energy and momentum in the reciprocal space. Micro- and nano-spot punctual and mapping experiments can be easily combined during a typical run of photoemission experiments in order to obtain in situ an averaged and nano-lateral discriminated information of the samples investigated. Thus, the recently inaugurated ANTARES end-station has proved the feasibility of an innovative instrument where precise nanoARPES determinations with accurate angular and linear displacements have been effectively combined with a well-focalized beam, precise mechanical scanning, and a high-resolution spectrometer. NanoARPES determinations can be completed with a direct imaging of core levels and their chemical shifts using X-ray photoemission with nano-lateral resolution. The good reproducibility and easy alignment of the ANTARES microscope have also made possible the detection of element-specific images of nano-objects like nano-wires and patterned samples.

Acknowledgements

We gratefully acknowledge the valuable support of the Engineering Service of SOLEIL, especially S. Lorcy and J.-L. Giorgetta for designing the nanoARPES microscope of ANTARES and F. Polack for the optical design of the ANTARES beamline. SOLEIL is supported by the Centre National de la Recherche Scientifique (CNRS) and the Commissariat à l'Energie Atomique et aux Energies Alternatives (CEA), France. ■

Note

Published with License by Taylor & Francis
© José Avila and María C. Asensio
This is an Open Access article distributed under the terms of the Creative Commons Attribution License (http://creativecommons.org/licenses/by/3.0), which permits unrestricted use, distribution, and reproduction in any medium, provided the original work is properly cited. The moral rights of the named author(s) have been asserted.

References

1. J. Avila et al., *Journal of Physics Conferences Series* **425**, 192023 (2013).
2. J. Avila et al., *Journal of Physics Conferences Series (SRI2012)* **425**, 132013 (2013).
3. T. Xu et al., *Phys. Rev. B* **81**, 115403 (2010).
4. J. Avila et al., *Sci. Rep*. **3**, 2438 (2013).
5. A.J. Marsden et al., *Physica Status Solidi-Rapid Research Letters* **7**(9), 643-646 (2013).
6. E. Moreau et al., *Phys. Rev. B* **88**, 075406 (2013).
7. J. Hass et al., *Phys. Rev. Lett.* **100**, 125504 (2008).
8. K.V. Emtsev et al., *Phys. Rev. B* **77**, 155303 (2008).
9. M. Sprinkle et al., *Phys. Rev. Lett.* **103**, 226803 (2009).
10. L.I. Johansson et al., *Sci. Rep.* **4**, 4157 (2014).

Future SRN Focus Topics

27.3	May/June	Industrial Applications
27.4	July/August	Detectors
27.5	September/October	Energy & Storage Research
27.6	November/December	Ultra-Low-Emittance Light Sources